Chemical Communications

Dynamic Article Links ►

Cite this: DOI: 10.1039/c0xx00000x

www.rsc.org/xxxxxx

Supplementary Information

Localised corrosion in Aluminium Alloy 2024-T3 using *in situ* TEM

Sairam Malladi*[a,b], Chenggang Shen[b], Qiang Xu[b], Tom de Kruijff[b], Emrah Yücelen[b,c], Frans Tichelaar[b], Henny Zandbergen[b]

DOI: 10.1039/b000000x

The details on specimen preparation, transfer, assembly of nanoreactor, experimental setup for *in situ* TEM studies and more details from the movie on *in situ* corrosion are presented here.

Materials and Methods:

The specimens used for this study have been prepared using an FEI Strata DB 235, dual-beam Ga focused ion beam - scanning electron microscope operated at 30 kV. The as-received AA 2024-T3 samples are strips of dimensions 100 X 200 X 0.8 mm^3. The surface preparation before FIB milling is carried out by mechanically polishing smaller squares of 10 X 10 mm using P 320, 600, 1200, 2400, 4000 SiC papers in the order mentioned. The final polishing is carried out by using 0.05 µm colloidal alumina suspension.

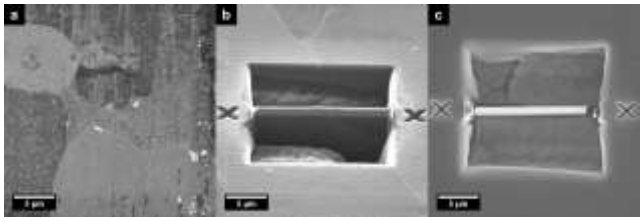

Fig. S1: FIB secondary electron images of: (a) AA 2024-T3 specimen revealing the grain boundaries after etching the surface layer by Ga ion milling; (b) an inclined image at 7° showing a cross-sectional FIB specimen, cut across a grain boundary, before final step of milling to thickness below 100 nm. (c) SEM image of the same FIB specimen after final thinning ≤ 100 nm thickness and releasing from the trench. This specimen is now ready for transfer.

The sample surface is then etched by focused Ga ion beam to reveal the grain boundaries, Fig. S1(a). The sample has an average grain size of 7 (±2) µm. As grain boundaries and precipitates are the locations where localised corrosion attack tends to initiate, cross-sectional specimens of dimensions 15 µm X 5 µm X 100 nm are cut across a grain boundary such that every TEM specimen has at least one grain boundary as shown in Fig. S1(b). After final thinning to thicknesses ≤ 100 nm, the specimen is cut at the edges and released from the trench, Fig. S1(c), and is ready for transfer. The specimen is transferred to the chip using an external micromanipulator with a glass capillary. Figures S2 (a-c) show the specimen lift-out and transfer onto the bottom chip of the nanoreactor.

The TEM specimens stick to the glass capillary by electrostatic force and when transferred on to a chip, the contact force between the Si_XN_Y membrane releases the specimen from the needle and adheres to the surface. Metallic specimens can be transferred within ~ 2 µm accuracy at reasonably high success rates (at least three out of five specimens can be transferred successfully).

The bottom half of the nanoreactor alone can be used for *in situ* heat-treatment experiments[1]. EDX mapping has been carried out on one such specimen in an FEI TITAN TEM equipped with ChemiSTEM™ technology (X-FEG, and Super-X detection system) [2] operated at 200 kV in STEM mode before assembling the nanoreactor.

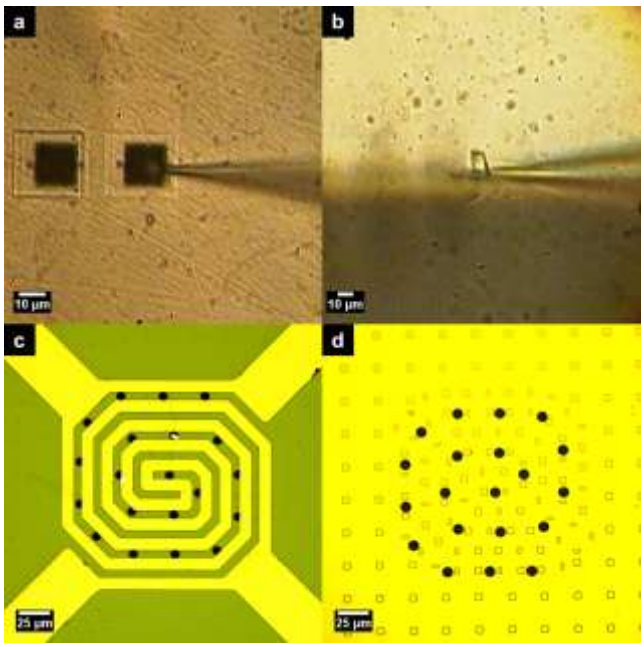

Fig. S2: Optical micrograph showing (a) two FIB specimens in a trenches, about to be transferred using an external micromanipulator with a glass capillary. The specimen in the right cavity is being lifted out of the cavity with the sharp glass needle (visible at the middle of the image from the right side). (b) Specimen removed from the trench and attached to the glass needle. (c) Specimens on thin membranes (dark circles) of the bottom chip of a nanoreactor, after successful transfer. (d) Central portion of the top chip showing the Si_XN_Y window and the thin membranes (dark circles).

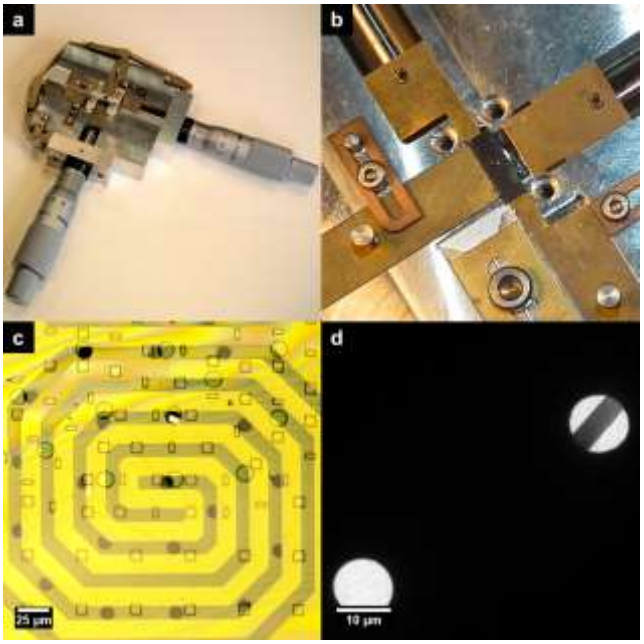

Fig. S3: (a) Alignment tool for aligning the top and the bottom chips under an optical microscope. (b) At the central portion of the alignment tool, the top chip is placed over the bottom chip with the Si_XN_Y windows facing each other. Also the sharp edges of phosphor-bronze plates attached to a calibrated screw to micrometre displacements. (e) Optical micrograph showing aligned thin membranes containing a specimen. (f) Low-magnification TEM image showing the specimen in an aligned nanoreactor.

After a successful specimen transfer, the bottom chip is placed in an alignment tool with top chip above it. The alignment tool is constructed in such a way that the top chip can be moved within 3-5 µm accuracy. Once the thin membrane(s) on the bottom and the top chip coincide, the top chip is clamped down applying a gentle force such that the chips remain aligned before gluing. Water glass (sodium silicate) which has set-time of around 45 min to 1 hour is used to glue the chips together in order to avoid any hydrocarbon contamination from glues. Once glued, the nanoreactor is ready for *in situ* TEM studies. To ensure assembling a working nanoreactor, the top as well as the bottom chips are tested to withstand 1 bar pressure before transferring a specimen.

The gas injection system for the *in situ* TEM studies is based on a simple gas cylinder bubbling through a reservoir containing the electrolyte (aqueous HCl of pH = 3) with a flow meter regulating the pressure and volume of the gas. Photographs of the gas injection system are shown in Fig. S4. Throughout the experiment a flow rate of 50 ml/min has been maintained. The *in situ* TEM experiments have been carried out on a Philips CM 30 T microscope operated at 200 kV.

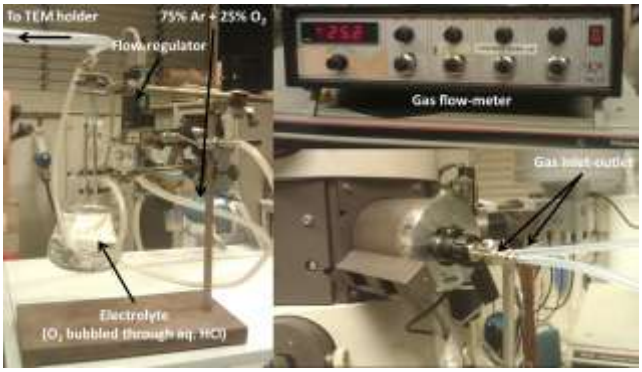

Fig. S4: Photographs showing the experimental setup. The image on the left shows $Ar+O_2$ gas being bubbled through a flask containing HCl of pH = 3. The gas coming out from the flask goes through another test-tube bubbler as a safety measure to prevent excess HCl entering the holder after topping up the flask. The volume of the gas flowing is regulated by a digital flow meter, connected in between the cylinder and the flask. For this experiment, a constant flow of 50 ml/min was maintained at a pressure of 1.5 bar. The image on the bottom right side shows the gas tubes connected to the holder inside the microscope.

More details from *in situ* TEM movies:

Only the most important features revealing localised corrosive attack at an anodic and cathodic precipitate have been emphasised in the main text. Here, more snapshots from the supplementary movie showing the other morphological changes are described.

Fig. S5 shows a comparison between the frame at the very beginning after injecting the reactive gas mixture into the nanoreactor and a frame after the gradual removal of the HCl droplets from the specimen surface. In this time frame, some changes are observed at the edges of the specimen. As the specimens used in this study are FIB specimens, artefacts such as the re-deposited material from milling at the bottom of the trench and the beam damaged area on the top side are observed. The beam damage on the top can be minimised by depositing a Pt protective layer but this has been avoided to prevent a galvanic couple between the Pt layer and the Al specimen. As these do not interfere with our primary areas of interest in the specimen (grain boundaries and precipitate-matrix interfaces), the changes occurring at the specimen edges have been ignored in this study.

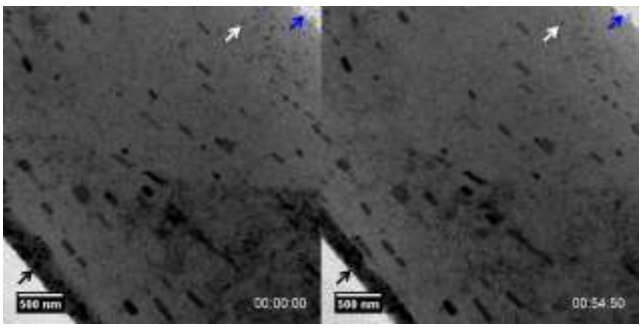

Fig. S5: Snapshots from the supplementary movie, the changes at the edges of the specimen are evident here, indicated by blue and black arrows. The diminished size of the aq. HCl droplets is quite evident.

A gradual decrease in the contrast of one of the grain boundary precipitate has been observed throughout the movie. This decrease in contrast is difficult to follow over the whole movie because there are also contrast changes in the Al matrix due to

diffraction contrast variations (orientation changes as small as 0.1° can cause this) and hence the exact moment when the attack on this precipitate has initiated cannot be determined accurately. This can possibly be avoided in future experiments by carrying out experiments in STEM-HAADF mode. Fig. S6 shows that after nearly 3 hours of exposure to the corrosive environment, some matrix etching has also initiated.

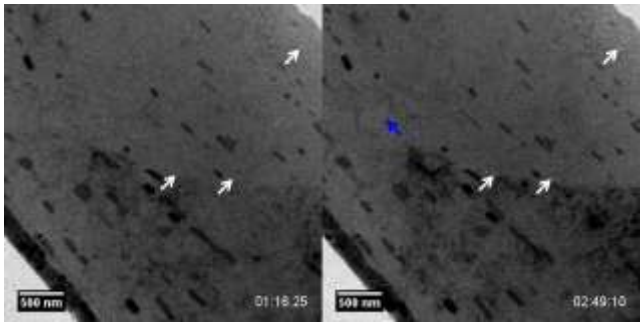

Fig. S6: In comparison with the image on the left, the image on the right shows the initiation of corrosion attack, signified by the bright spots next to the white arrows is evident. Also surface etching of the aluminium matrix is visible next to the blue arrow.

One of the challenges with *in situ* experiments is the unpredictability of events. From the quasi *in situ* experiments, we expected the initiation of corrosion attack within an hour, however, the experiment lasted longer and hence the HCl reservoir had to be refilled after 3 hours. Fig. S7 shows the reappearance of HCl droplets similar to the ones observed at the very beginning of the video. Further to these changes, significant morphological changes have been observed in the specimen. This can possibly be due to difference in the saturation levels of reactive gas mixture during the *quasi in situ* and *in situ* experiments, differences in the size of the flow channel and most importantly the constant illumination of the electron beam.

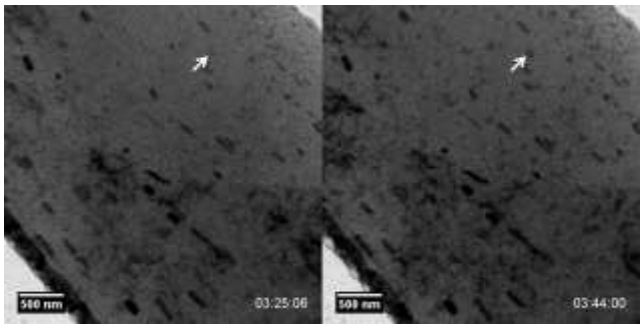

Fig. S7: Here the development of HCl droplets after refilling the HCl reservoir is shown

Furthermore, the electron beam could induce a negative charge on the aluminium specimen surface, an effect similar to cathodic polarization, which can cause a resistance to corrosive attack. On the other hand, the electron beam could also dissociate HCl to its respective ions, resulting in making aluminium susceptible to corrosion by Cl^- which is well documented[3, 4]. Therefore, there are two counterbalancing effects under the electron beam. There is a good possibility that an enhanced corrosion attack is witnessed after the HCl has been refilled due to the aforementioned reason. This calls for more studies on optimizing a controllable gas-liquid environment and as well as understanding the electron beam effects, which is beyond the scope of this article.

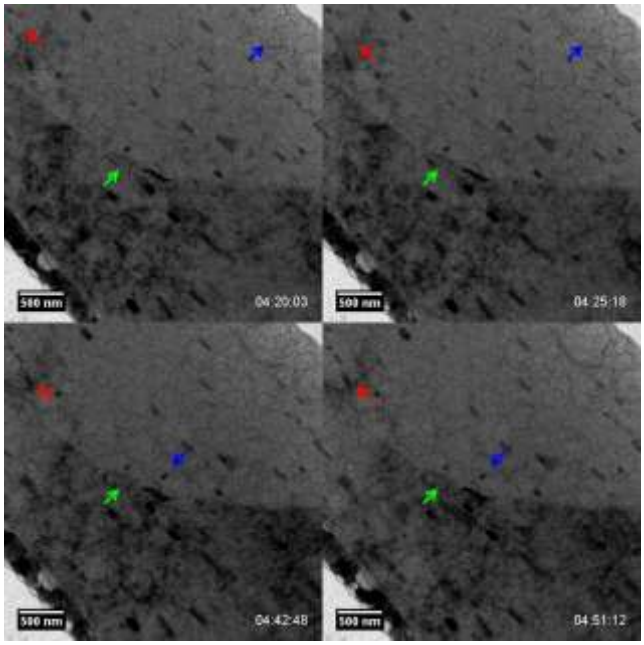

Fig. S8: Progression of corrosion attack at a grain boundary precipitate, as well as in the matrix.

In Fig. S8, the image on the top left shows the grain boundary precipitate next to the green arrow has a significantly diminished intensity compared with the previous images, while attack in the matrix is also observable next to the red and the blue arrows. In the next image on the top right, the matrix attack next to the intermetallic precipitates has progressed further as indicated by the red arrow while the matrix etching next to the blue arrow is more evident. In the image on the bottom left, the matrix attack next to the red arrow has progressed further but the most noticeable feature is the formation of the dark particle next to the blue arrow. In the image on the bottom right, obtained at the very end of the movie, the matrix etching is significant. On comparing the top two images with the bottom two images, the intensity of the grain boundary precipitate shown by the green arrow seems to have diminished significantly along with the formation of the dark particle next to the blue arrows.

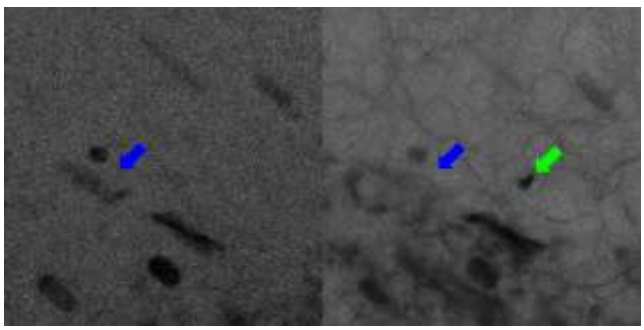

Fig. S9: Bright field images obtained before and after the corrosion experiments reveal the removal of grain boundary precipitate next to the blue arrow and the formation of a dark feature next to the green arrow (also shown as Figures 3(c) & (d) in the main text).

The dark contours, as visible in the Fig. S9 around the precipitate could be corrosion products from the precipitate while the dark particle shown by the green arrow could be the remnant material from de-alloyed matrix. These questions can be answered by combining the experiments with *in situ* elemental mapping.

Notes and references

1. M. A. van Huis, N. P. Young, G. Pandraud, J. F. Creemer, D. Vanmaekelbergh, A. I. Kirkland and H. W. Zandbergen, Adv. Mater., 2009, 21, 4992-4995.
2. P. Schlossmacher, D. O. Klenov, B. Freitag and H. S. von Harrach, Microscopy Today, 2010, 18, 14-20.
3. V. Guillaumin and G. Mankowski, Corrosion Science, 1999, 41, 421-438.
4. R. T. Foley, Corrosion, 1986, 42, 277-288.